International Journal of Engineering Research and Development
e- ISSN: 2278-067X, p-ISSN: 2278-800X, www.ijerd.com
Volume 22, Issue 6 (June 2026), PP 80-91

Dynamic Response of Ballasted Track Bed–Subgrade Systems in Seasonally Frozen Regions under Coupled Effects of Train Speed and Ice Content

Yin Zhang[1], Zhongchang Wang[1*], Hongrui Liu[1], Yanhao Liu[1], Qinghui Zhu[1]
[1] *School of Transportation Engineering*
Dalian Jiaotong University, Dalian, 116028, China
Corresponding Author: Zhongchang Wang.

ABSTRACT: *Ballasted track beds of high-speed railway subgrades in seasonally frozen regions are highly susceptible to performance degradation under the combined actions of train dynamic loads and water-ice phase changes. To address this, a bidirectional two-dimensional coupled discrete element-finite difference (DEM-FDM) numerical model was developed to systematically investigate the dynamic responses and micromechanical mechanisms of the ballast-subgrade system under coupled operational scenarios with varying train speeds (80–200 km/h) and ballast ice contents (0%–30%). The results demonstrate that the vertical displacement of the ballast bed is governed by the antagonistic effects of speed-induced nonlinear amplification and ice-matrix-induced suppression, with high ice contents effectively locking the particle fabric in regions far from the loading zone. While the unfrozen ballast bed exhibits a flexible, diffusion-type load transmission characterized by a broad trapezoidal distribution, the pore ice in the frozen ballast restricts particle sliding, forcing the path to evolve into a rigid, concentrated strong force chain network. Consequently, the loads penetrate deeply into the subgrade in a narrow columnar pattern, synergistically amplifying the subgrade dynamic stress by a factor of 2.0–2.5. Within the core loading zone of the subgrade, the vertical dynamic stress is approximately 6–8 times the lateral component and exhibits a distinct "central-high, peripheral-low" spatial distribution, rendering it considerably more sensitive to frost heave and thaw weakening. This study provides critical scientific guidance for the structural design, operation, and maintenance of ballasted tracks in cold regions.*

Key words: *Ballasted track bed; High-speed railway; Seasonally frozen regions; Coupled DEM-FDM model; Train speed; Ice content*

Date of Submission: 05-06-2026 Date of acceptance: 16-06-2026

I. INTRODUCTION

The rapid expansion of high-speed railways and increasing train speeds have intensified serviceability problems of ballasted tracks in seasonally frozen regions[1]. Under cyclic train loading, ballast beds are prone to cumulative deformation, leading to ballast degradation, fouling, and subgrade mud-pumping. In freeze–thaw environments, dynamic ice-content evolution further deteriorates ballast performance: freezing weakens granular interlocking through ice crystal growth, while thawing reduces bearing capacity due to excess pore water pressure. The coupling of freeze–thaw damage and dynamic train loading is therefore the key mechanism governing ballast deterioration in cold regions[2].

Extensive studies have investigated the mechanical behavior of ballast materials. Lim et al.[3] conducted static crushing tests on ballast particles and applied the Weibull distribution to characterize strength and size effects, while Yan et al. [4] analyzed the relationship between crushing strength and particle size. Subsequent studies focused on low-temperature effects in frozen regions. Laboratory experiments by Li et al. [5] and Wang et al. [6] confirmed that ice content controls the strength evolution and frost-heave behavior of frozen ballast. Liu et al. [7] further revealed the influence of temperature on compressive strength through uniaxial compression tests. At the mesoscopic level, Bian et al. [8] proposed a DEM-based “water–ice phase change expansion” model to capture freeze–thaw-induced micro-damage and structural degradation. However, particle-scale studies cannot fully explain the macroscopic response of ballast beds under coupled frost heave and train loading. Recognizing this limitation, Nurmikolu [9] performed low-temperature field tests in Finland and demonstrated that freezing significantly alters the dynamic response of ballasted tracks. Liu et al. [10] and Bian et al. [11] further clarified the freezing-induced increase in ballast stiffness and attenuation of elasticity, as well as the associated stress transmission characteristics. Li [12] and Chen et al. [13] investigated the evolution of cumulative settlement and dynamic response under combined freezing and cyclic loading. Considering the strong ballast–subgrade interaction, Ren et al. and Bian et al. [14,15] established coupled DEM–FDM ballast-subgrade models, which

realistically reproduce boundary constraints and deformation compatibility, providing an effective framework for evaluating ice-content effects.

Despite these advances, three major limitations remain: (1) train speed and ice content are usually studied independently, and their coupled effects on ballast dynamics and contact evolution remain unclear; (2) ballast–subgrade interaction is often oversimplified, limiting accurate simulation of stress states; and (3) spatial variations of dynamic responses along critical load paths are insufficiently quantified, hindering the identification of weak zones prone to damage.

To overcome these limitations, this study develops a refined 2D coupled DEM–FDM model to investigate the combined influence of train speed and ice content on ballast–subgrade systems. The study systematically quantifies the spatial characteristics of displacement, acceleration, and stress responses, while revealing the nonlinear evolution of deformation compatibility and dynamic transmission mechanisms under coupled speed–ice-content conditions.

II. Establishment of numerical models

2.1 Discrete Element-Finite Difference Coupling Model for Ballast-Subgrade

Based on the geometric features of ballast particles, this study introduces high-precision photogrammetry technology (Reality Capture) to capture the authentic surface micro-morphology and contour information of ballast grains through multi-view image acquisition and digital processing. The acquired contour data were exported as .dxf files and subsequently imported into the computer environment utilizing the geometry module of the PFC software. Finally, a rigid block algorithm was applied to generate the ballast cluster models embedded with realistic geometric features, with the complete modeling workflow illustrated in Figure 1(a). In accordance with the "Railway Ballast" standard (TB/T 2140—2018), the grain size distribution curve of Grade I crushed stone ballast from existing high-speed railway lines was adopted, as shown in Figure 1(b). The geometric dimensions and structural configurations of the ballasted track bed were determined with reference to typical high-speed railway design codes. Ballast particle clusters were generated using the built-in FISH functions of the discrete element software, and the assembled model comprises approximately 1,700 ballast grains varying in size and shape. In the model, the sleeper was simplified as a rectangular rigid body. To apply dynamic loads, five rigid spheres were arranged on each side above the sleeper to represent the rails. The discrete element model of the ballasted track bed is depicted in Figure 1(c), and its micromechanical parameters are summarized in Table 1(a).

Owing to the dense and homogenous compaction of the railway subgrade and foundation soils, they exhibit typical continuum mechanics characteristics. Consequently, within the continuum mechanics framework, a coupled subgrade-foundation model was established using the finite difference program FLAC. The model incorporates distinct structural layers, including the subgrade surface layer, subgrade bottom layer, subgrade body, foundation, and bilateral reinforcement zones. Given that this study focuses on the transient dynamic response of the ballast bed under train dynamic loads, the materials of all layers were generalized as isotropic linear elastic media. Their physical and mechanical parameters are summarized in Table 1(b).

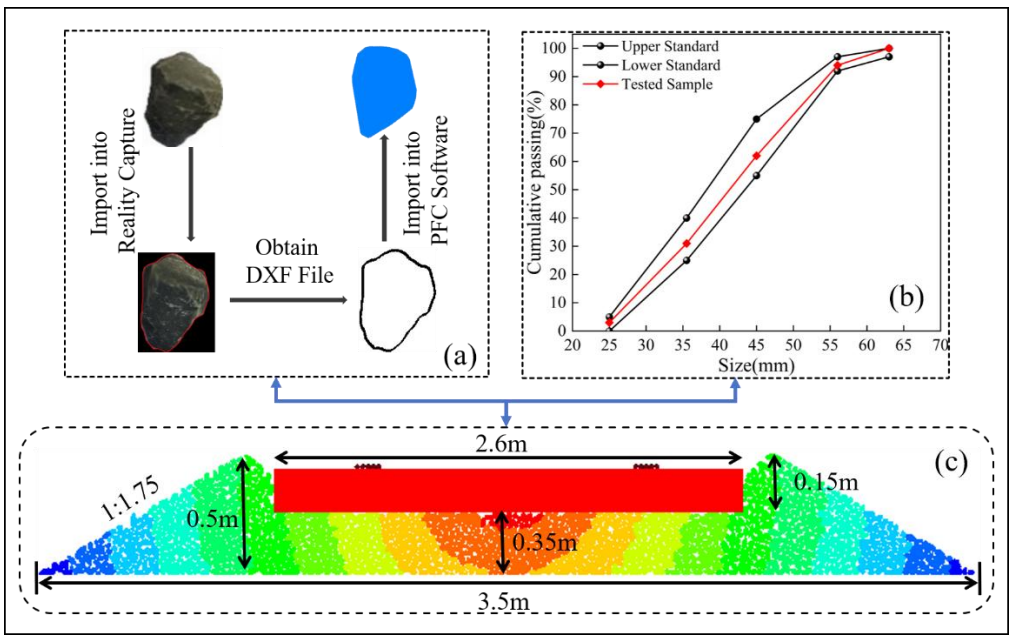

Figure 1: Discrete element model of ballasted track bed

Table 1: Model mechanical parameters

(a) Mesoscopic Mechanical Parameters of Ballast Bed	
Parameter	Value
Ballast density /kg·m^3	2700
Sleeper density /kg·m^3	3025
Normal/tangential contact stiffness between ballasts / (N·m^{-1})	3.2e8
Normal/ tangential contact stiffness between ballasts and sleepers / (N·m^{-1})	5.0e8
Normal contact stiffness between sleepers and rails / (N·m^{-1})	1.373e12
Tangential contact stiffness between sleepers and rails / (N·m^{-1})	5.529e11
Friction coefficient of rai ballast	0.7

(b) Subgrade Physical and Mechanical Parameters Table				
Material	Poisson's Ratio	Elastic Modulus (MPa)	Thickness (m)	Density (kg/m^3)
Subgrade bed surface layer	0.25	10×10^5	0.4	1.9×10^5
Subgrade bed bottom layer	0.25	10×10^5	0.6	1.8×10^5
Main subgrade body	0.3	15.5×10^5	5	1.75×10^5
Foundation	0.35	0	6	1.75×10^5
Lateral reinforcement zones	0.6	10×10^3	10	2×10^4

To comprehensively analyze the dynamic response of the ballasted track bed-subgrade system under high-speed train dynamic loading, a coupled ballasted track bed-multi-layered subgrade model is developed based on the numerical coupling concept of the discrete element method (DEM) and the finite difference method (FDM). The upper part of the model consists of the ballasted track bed established using DEM, while the lower part comprises the multi-layered subgrade modeled by FDM. The coupling is achieved through shared boundary nodes and contact elements, ensuring continuity of force and displacement at the interface, thereby enabling bidirectional transfer of train-induced dynamic loads between the granular and continuum media.

The coupling process must adhere to the following core requirements: geometrically, the coupling walls in FDM serve as boundary elements/interfaces, and the boundary particles in DEM maintain consistent position and shape; in terms of force transfer, the contact forces between DEM particles and the coupling walls are transmitted to the corresponding FDM nodes; for displacement feedback, the nodal displacements from FDM are fed back to DEM through the coupling walls as boundary motion conditions. Bidirectional interaction is performed at each time step to ensure consistent mechanical behavior. This model achieves an effective integration of the particle-scale and continuum-scale approaches, capturing the nonlinear contact, sliding, and rearrangement characteristics among ballast particles, and accurately describing the overall deformation and stress propagation laws of the subgrade soil. The DEM-FDM coupled model of the ballasted track bed-subgrade system is shown in Figure 2.

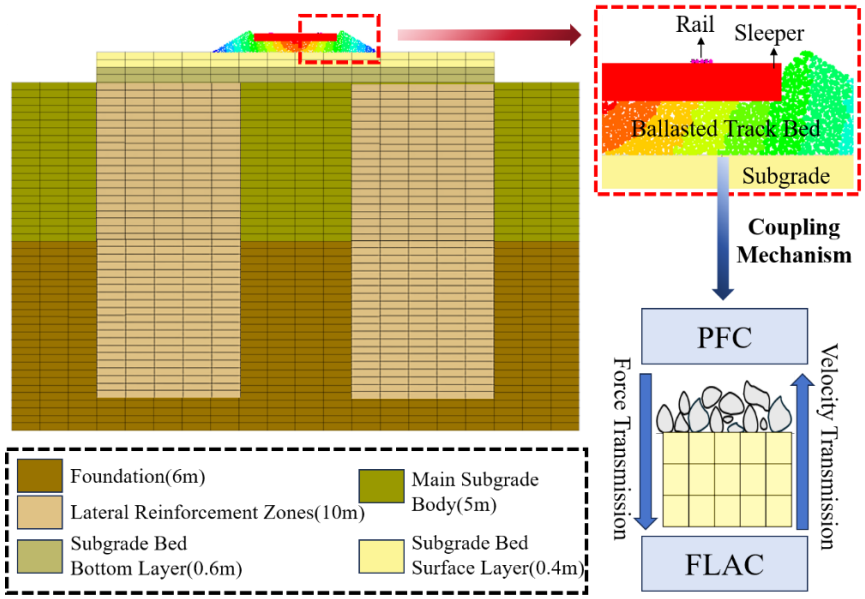

Figure 2: Discrete Element-Finite Difference Coupling Model for Ballast-Subgrade

2.2 Frozen Ballast Bed Model

The mesoscopic mechanism of the frozen ballast bed relies on the pore water freezing to bond the granular ballast into a coherent skeleton. In this study, the ballast particles are simulated as block elements, and small spherical particles (balls) are filled into the skeletal voids to represent the pore ice. To capture the freezing effects of the track bed, the parallel bond model is employed to characterize the contact behaviors at both the ice-ballast and ice-ice interfaces. Once the contact forces satisfy the criteria defined in Eq. (1), the bonds rupture, sequentially leading to the initiation of shear or tensile micro-cracks.

$$\begin{cases} |F_n| > |F_n^C| \\ |F_s| > |F_s^C| \end{cases} \tag{1}$$

Where F_n and F_s are the normal and shear contact forces, respectively, and F_n^c and F_s^c denote the normal and shear bond strengths.

The linear contact model was adopted for contacts between ballast particles and between particles and walls. The normal and shear contact forces are calculated as:

$$F_n = K_n \Delta\delta_n \tag{2}$$

$$F_s = K_s \Delta\delta s \tag{3}$$

where F_n is the normal contact force (positive in compression), K_n is the normal contact stiffness, $\Delta\delta_n$ is the normal overlap between particles, F_s is the shear contact force, K_s is the shear contact stiffness, and $\Delta\delta_n$ is the shear displacement increment. Sliding occurs when $F_s > \mu F_n$, where μ is the interparticle friction coefficient.

The localized frozen ballast bed model is illustrated in Figure 3. The volumetric ice content of the specimen is specified as 10%. The model dimensions comprise a frozen ballast assembly with a length of 0.15 m and a height of 0.15 m, wherein the size of the embedded ice elements ranges from 1.0 to 1.1 mm. The specific micromechanical parameters of the frozen ballast bed are summarized in Table 2.

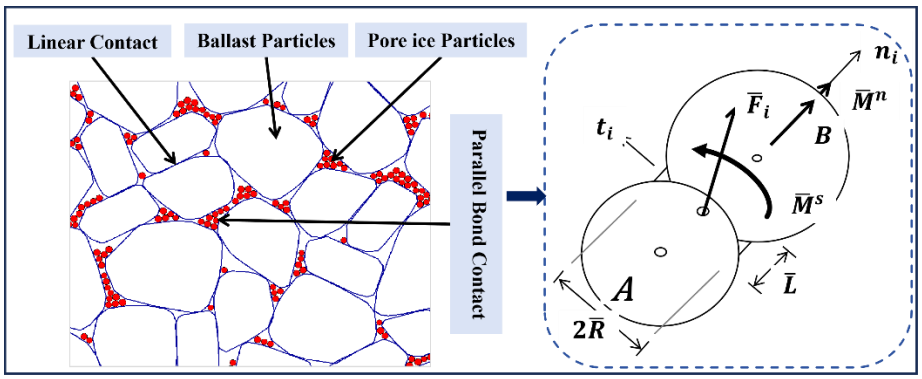

Figure 3: Local Model of Frozen Ballast Bed

Table 2: Mesoscopic Parameters for Frozen Subgrade

Parameter	Value
Minimum ice particle radius / (mm)	1.0
Maximum ice particle radius / (mm)	1.2
Ice particle density / (kg/m3)	917
Ice interparticle friction coefficient	0.0
Ice parallel bond strength / (MPa)	0.2

2.3 External Load Input for Coupled Model

The definition of train dynamic loading is the most critical boundary condition for reliable dynamic track simulations. To accurately reflect the dynamic effects during train passage, this study adopts a quasi-static superposition with dynamic amplification method to determine the dynamic load on the sleepers. Based on the classical theory of track dynamics, the dynamic pressure R_d acting on the sleeper can be expressed as the product of the static pressure on the sleeper R_0, the speed amplification factor α, and the eccentric load factor β [16]:

$$R_d = R_0 (1 + \alpha + \beta) \tag{4}$$

Among them, the static pressure on the sleeper R_0 is calculated based on the given axle load (15.85 t) and the wheel load distribution ratio (34%). For straight track, the eccentric load factor β=0. The speed factor α is

determined according to the specification: when the running speed $V \leqslant 160$km/h, $\alpha=0.6V/100$; when $V>160$km/h, $\alpha=1.0$ is adopted.

To simulate the dynamic fluctuations caused by the periodic passage of trains, the above dynamic pressure R_d is taken as the reference amplitude F_0 and applied to the rail-bearing position of the sleeper in the form of a harmonic function[17]:

$$F_t = -F_0\left(1+\sin\left(2\pi ft-\pi/2\right)\right) \tag{5}$$

where f is the loading frequency. Based on the relationship between typical bogie fixed wheelbase and train speed, a uniform value of 10 Hz is adopted in this study.t is the loading time. For the four designated train speed conditions of 80km/h、120km/h、160km/h and 200km/h, the corresponding calculated sleeper dynamic pressure amplitudes are 3.91 kN, 4.54 kN, 5.18 kN, and 5.29 kN, respectively.

2.4 Validation of the Discrete Element Mode

To validate the developed discrete element model, a numerical analysis was performed focusing on the dynamic response of a sleeper under train-induced loading. The CRH2 Electric Multiple Unit (EMU), characterized by an axle load of 14 t and an operating speed of 160 km/h, was selected as the reference train. Figure 4 illustrates the vertical displacement time-history curve of the sleeper under periodic train loading. As shown in the figure, the peak dynamic displacement of the sleeper is approximately 0.35 mm, and the vibration exhibits stable, distinct periodic characteristics. The numerical results are in excellent agreement with the average field-measured sleeper displacement of 0.39 mm obtained from the Hefei-Wuhan Passenger Dedicated Line [18]. This close agreement confirms that the developed DEM model can accurately replicate the dynamic response of the ballasted track system under realistic operating conditions.

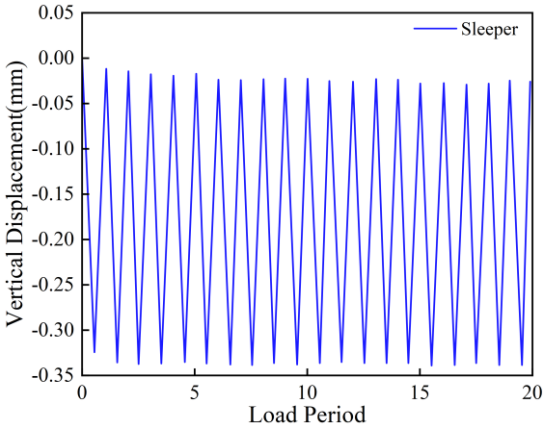

Figure 3: Dynamic Displacement Time History Curve of Sleeper

2.5 Monitoring Point Arrangement

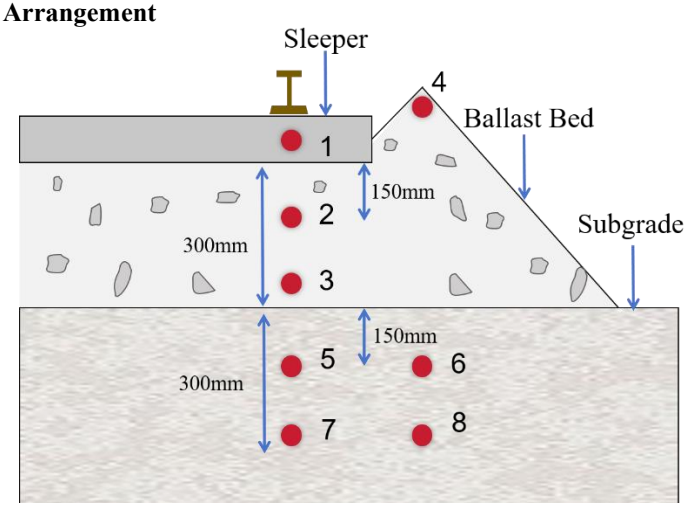

Figure 4: Layout of Monitoring Points in Ballast and Subgrade

To systematically observe and analyze the vibration characteristics at typical positions, measurement points are arranged within the established discrete element model of the ballasted track bed (see Figure 4).

Considering the freezing conditions, rational layout of monitoring points is executed to reveal the vibration propagation and attenuation characteristics across distinct regions of the ballast bed and the subgrade layer under complex operational scenarios. Specifically, Points 1 is located at the sleeper level; Points 2 and 3 are positioned at depths of 150 mm and 300 mm beneath the sleeper bottom, respectively, both aligned directly beneath the rail seat; Point 4 is situated at the crest of the ballast shoulder. Within the subgrade section, four monitoring points are deployed: Points 5 and 7 are aligned directly beneath the rail seat, positioned at depths of 150 mm and 300 mm below the ballast bottom, respectively; meanwhile, Points 6 and 8 are located directly below Point 4 at the crest of the ballast shoulder.

III. Results and Discussion

To systematically elucidate the influential mechanisms of train speed and ice content on the dynamic behavior of the ballast-subgrade system, this chapter utilizes the validated two-dimensional (2D) coupled discrete element-finite difference model to conduct numerical simulations across combined operational scenarios, incorporating variations in train speed (80, 120, 160, and 200 km/h) and ballast ice content (0%, 10%, 15%, 20%, 25%, and 30%).

3.1 Macroscopic Dynamic Response Characteristics Under the Interaction of Vehicle Speed and Ice Content

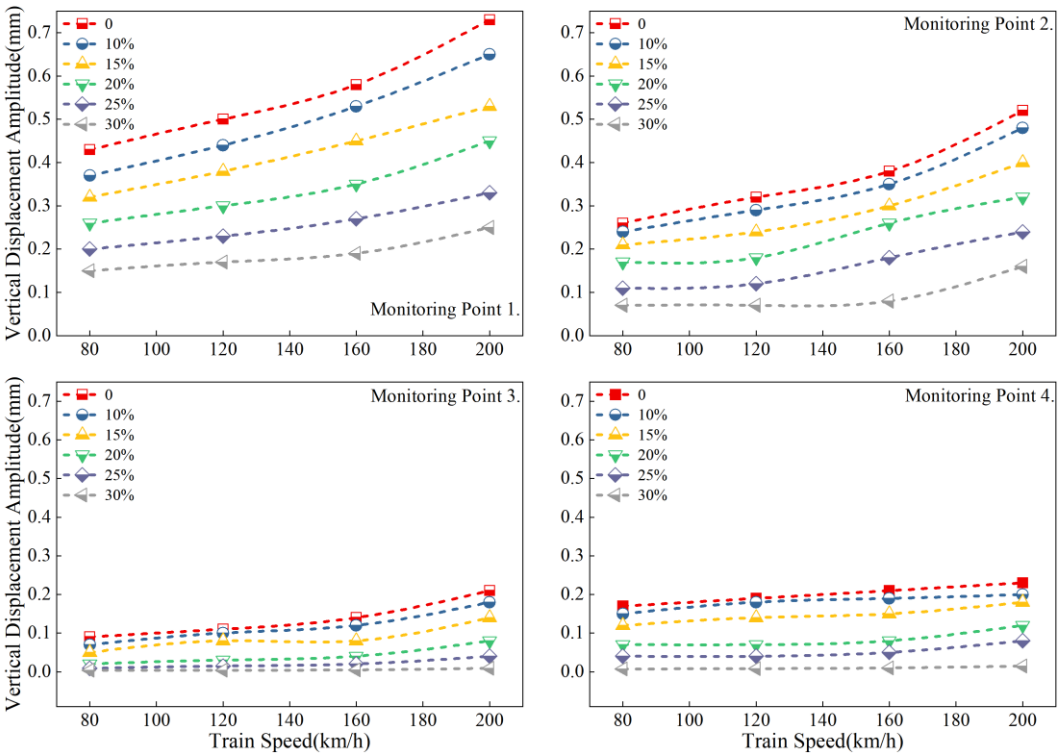

Figure 5: Curves of Vertical Displacement Amplitude of Ballast Bed Under the Interaction of Different Train Speeds and Ice Contents

Figure 5 illustrates the vertical displacement amplitudes of the ballast bed under the interactive effects of varying train speeds and ice contents. The following key observations are drawn from the coupled analysis:

(1) Antagonistic effects of speed amplification and ice-induced suppression. Vertical displacement at all monitoring points is positively correlated with train speed and negatively correlated with ice content. Train speed exerts a positive amplification effect on displacement, with a sharp, nonlinear increase observed once the speed exceeds 160 km/h. Conversely, ice content acts as a strong inhibitory factor. As ice content increases, the global stiffness and interparticle cementation of the ballast bed are enhanced, leading to a significant reduction in displacement amplitudes. Notably, this suppressive effect becomes increasingly pronounced with greater burial depths.

(2) Spatial heterogeneity of "weak attenuation near the load, strong attenuation far from the load." The ice-bonding effect strengthens the interparticle connection forces and the overall stiffness of the ballast assembly, effectively inhibiting relative particle sliding and reducing vertical displacement. This process generates a distinct spatial heterogeneity in vibration attenuation. The near-sleeper region directly bears the heavy train

dynamic loads, which limits the restrictive effect of the ice matrix, thereby maintaining high vibration resistance. In contrast, the ice-induced confinement is highly effective in deeper and peripheral (shoulder) zones, where displacement amplitudes drop drastically. Overall, high ice contents (≥20%) can significantly enhance the global dynamic stability of the ballasted track bed by locking the particle fabric in these peripheral and deep regions.

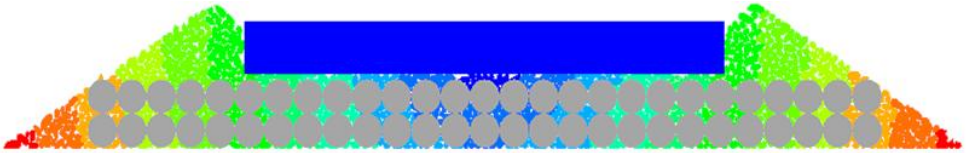

Figure 6: Layout Diagram of Measurement Circles at the Ballast Bed Monitoring Points

To systematically capture the vertical stress distribution at various lateral positions of the ballast bed under train dynamic loads, a layered stress monitoring array was deployed inside the ballast assembly. Two monitoring layers were established at depths of 100 mm (near-sleeper zone) and 250 mm (far-sleeper zone) below the sleeper bottom to facilitate a comparative analysis of internal load transfer characteristics. As illustrated in Figure 6, the system comprises 54 circular stress sensors (160 mm in diameter) embedded in a matrix configuration across the ballast bed cross-section to comprehensively capture the stress field distribution and evolution within the core loading zone.

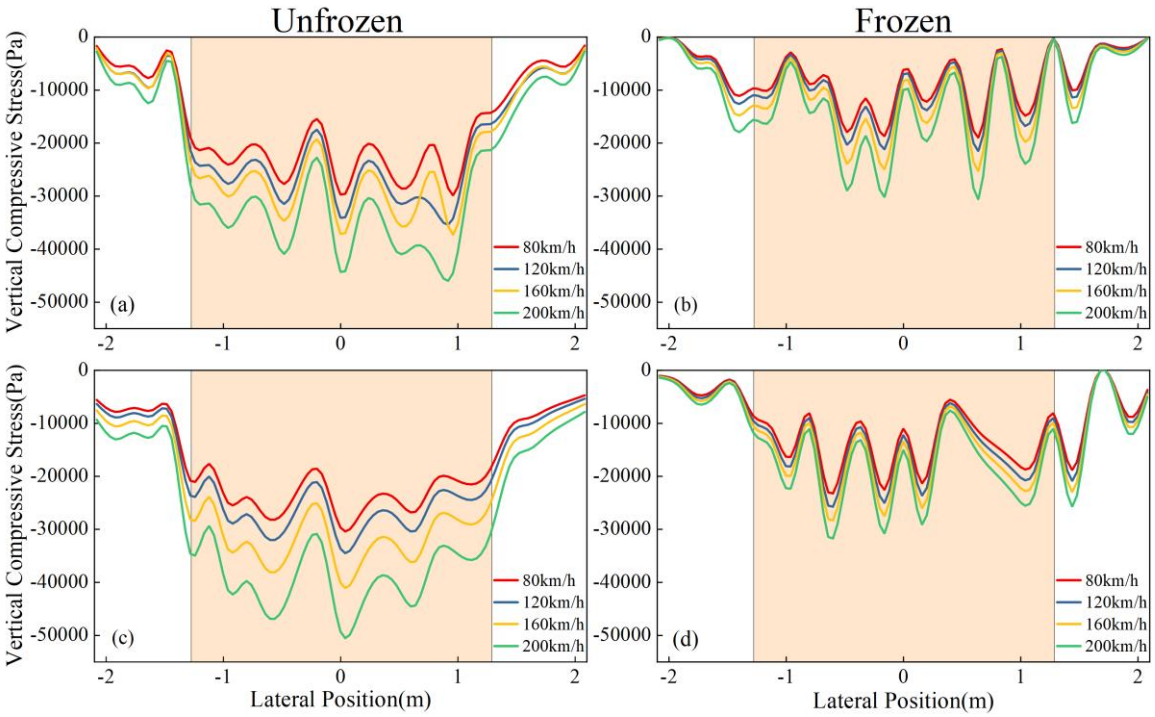

Figure 7: Spatial Distribution of Vertical Dynamic Stress in Ballast Bed

Figure 7 illustrates the spatial distribution of vertical compressive stress within the ballast bed at depths of 100 mm and 250 mm beneath the sleeper under different train speeds and freezing conditions. The results reveal that vertical stress exhibits a distinct nonuniform multi-peak distribution, with the maximum stress concentrated beneath the sleeper and gradually attenuating toward the ballast shoulders. Increasing train speed significantly amplifies the stress magnitude, whereas frozen ballast demonstrates lower stress growth rates than the unfrozen condition.

Freezing fundamentally alters the internal load-transfer mechanism of the ballast bed. In the shallow layer (100 mm depth), ice bonding suppresses particle rearrangement and lateral stress diffusion, resulting in stronger local stress concentration and steeper attenuation gradients. In contrast, at greater depth (250 mm), the ballast assembly exhibits a more distributed stress-transfer pattern due to granular stress redistribution, indicating that the freezing effect weakens progressively with depth.

Moreover, the stress amplification induced by train speed is considerably more pronounced in unfrozen ballast, where particle sliding and rearrangement dominate the transmission process. Under frozen conditions, the ice-cemented particle skeleton enhances the global stiffness of the ballast bed and restrains stress propagation, thereby mitigating the sensitivity of vertical stress to train speed. This suppression effect becomes increasingly significant in deeper regions, where the frozen ballast behaves more as a stress-buffering layer than a direct rigid load path.

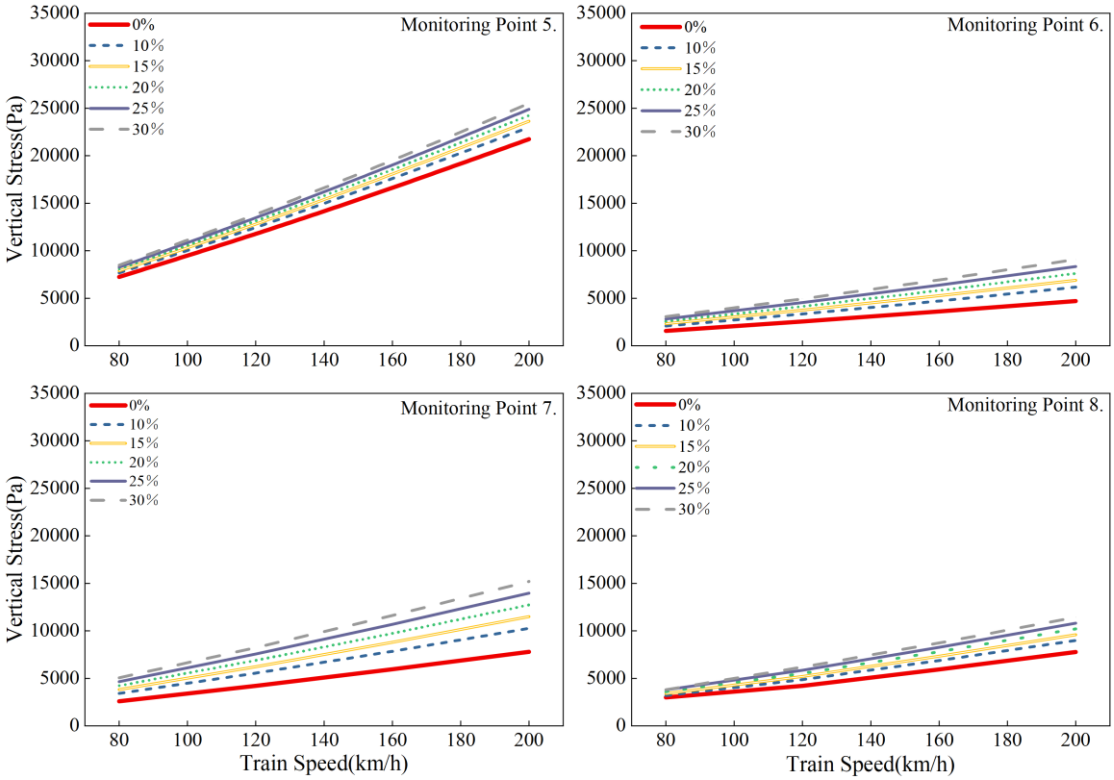

Figure 8: Curves of Vertical Stress of Subgrade Under the Interaction of Different Train Speeds and Ice Contents

Figure 8 presents the vertical stress response of the subgrade under varying train speeds and ice contents. Two key findings are observed:

(1) Train speed governs dynamic stress amplification. Under constant ice content, vertical dynamic stress increases monotonically with train speed. As speed rises from 80 km/h to 200 km/h, stress amplitudes increase by approximately 2.0–2.5 times. Stress remains highest in the central loading zone and decreases toward lateral and deeper regions, forming a characteristic “central-high, peripheral-low” distribution.

(2) Ice content enhances stress transmission. Vertical stress at all monitoring points increases with ice content, indicating that freezing improves ballast stiffness and load-transfer efficiency. Train speed and ice content jointly amplify vertical stress, although speed remains the dominant factor. The strengthening effect of ice content is more evident at deeper and peripheral locations, suggesting that freezing preferentially stiffens stress transmission paths away from the direct loading zone.

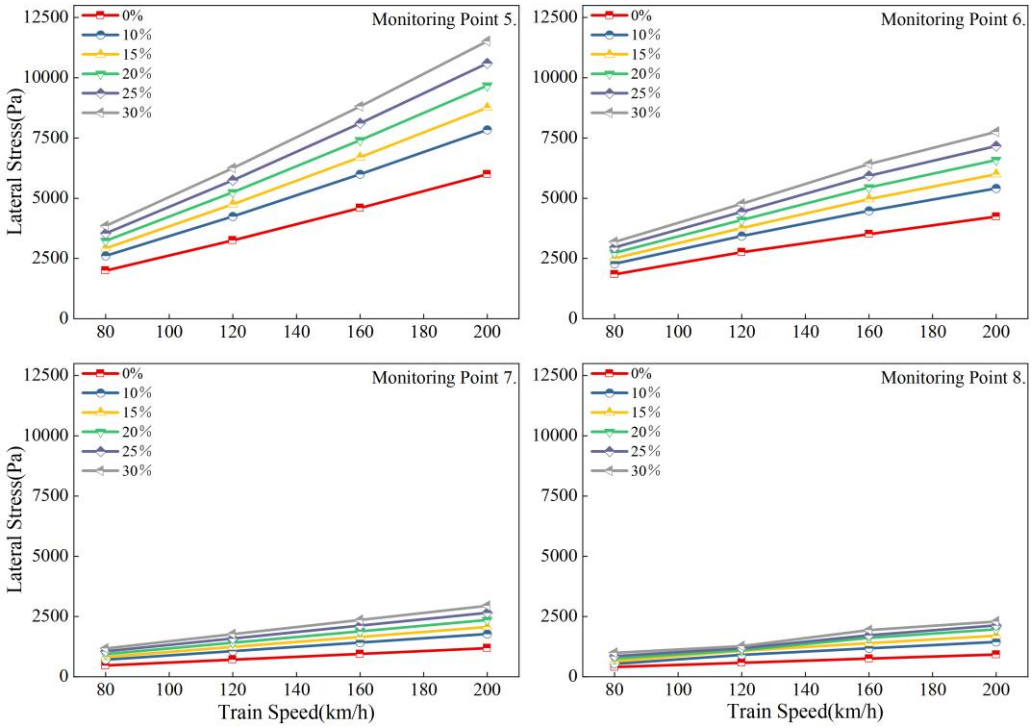

Figure 9: Curves of Lateral Stress of Subgrade Under the Interaction of Different Train Speeds and Ice Contents

Figure 9 illustrates the lateral stress response of the subgrade under the interactive effects of train speed and ice content. Two principal observations emerge:

(1) Monotonic amplification of lateral stress with pronounced ice content sensitivity.

Lateral stress in the subgrade increases monotonically with both train speed and ice content, with ice content demonstrating a particularly pronounced amplification effect. The lateral stress amplitudes at Points 5 and 6 (shallow zone directly beneath the rail) are substantially higher than those at deeper Points 7 and 8, indicating that the coupled action of frost heave and dynamic loading is primarily concentrated within the shallow subgrade layers.

(2) Vertical stress dominance and contrasting mechanistic responses.

The increase in vertical dynamic stress is significantly greater than that in lateral stress; in the core loading zone, vertical stress is approximately 6–8 times the lateral stress, confirming that vertical loading dominates the overall stress distribution. The two stress components exhibit markedly different response mechanisms to changes in ice content, with vertical stress being more sensitive to frost heave. Accordingly, vertical stress serves as the key indicator for stability assessment of subgrades in cold regions, and particular attention should be paid to stress concentrations beneath the rails and to lateral stress growth during design and operational monitoring.

3.2 Meso-scale Force Transmission and Response Mechanism under Typical Working Conditions

Based on the parametric analysis, a representative case with a train speed of 160 km/h and an ice content of 30% was selected to investigate the meso-scale load transfer mechanisms and particle dynamics in unfrozen and frozen ballast beds. Figure 10 shows the spatial distribution of inter-particle contact force vectors under train loading, where sphere size and color indicate contact force magnitude. The main observations are as follows:

(1) **Unfrozen ballast exhibits flexible load diffusion**. Contact forces form a trapezoidal distribution that gradually attenuates from the sleeper downward, while force chains spread uniformly through the ballast layer. Multi-directional particle contacts create a stable mechanical network that disperses concentrated loads and reduces local particle breakage, thereby maintaining both load-bearing and vibration attenuation performance.

(2) **Frozen ballast exhibits rigid concentrated load transfer**. Ice bonding restricts particle sliding and rearrangement, forming rigid force chains that transmit loads directly to the subgrade in a nearly rectangular pattern with stronger vertical stress concentration. Contact forces increase significantly near ice-cluster boundaries and at the ballast–subgrade interface, raising the risk of particle breakage and structural damage. In addition, ice-bonded clusters hinder lateral stress diffusion, further intensifying local force concentration.

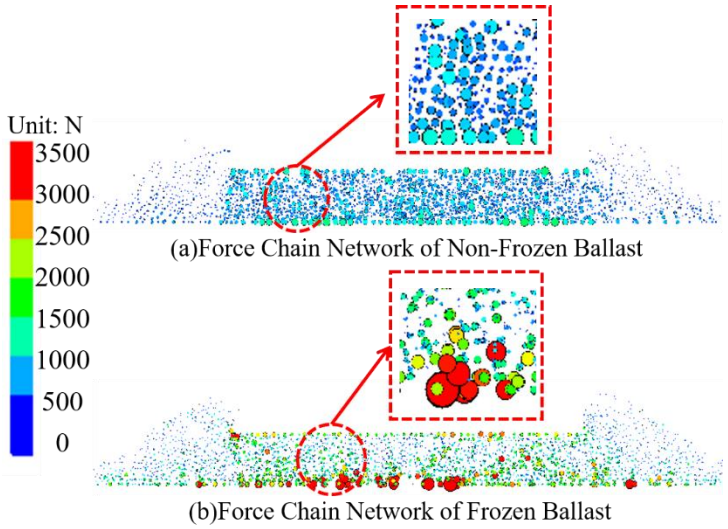

Figure 10: Force Chain Network of Unfrozen and Frozen Ballast Under Load

Figure 11 presents the particle motion states of granular and frozen ballast beds under peak loading. The results indicate that:

(1) The mechanical response of the granular ballast bed is governed by the flexible diffusion of particle force chains. Ballast particles beneath the sleeper exhibit predominantly vertical displacement, which attenuates progressively with depth and reaches its maximum at the sleeper-ballast interface. The displacement field shows an approximately trapezoidal distribution, with notable horizontal displacements occurring at the shoulder due to insufficient lateral confinement.

(2) In contrast, the frozen ballast bed is dominated by stiffness partitioning and heterogeneous deformation. Freezing substantially increases the overall stiffness, confining deformation primarily to the shallow layer (0–15 cm) beneath the sleeper. Ice cementation induces spatially heterogeneous stiffness, with higher rigidity at the sleeper center than at the shoulder. The displacement contours of the frozen ballast display a bimodal distribution, in contrast to the unimodal pattern observed in the unfrozen case. Although freezing enhances the bearing capacity, it alters the stress transmission path, transforming the deformation mode from diffusive attenuation to zoned confinement.

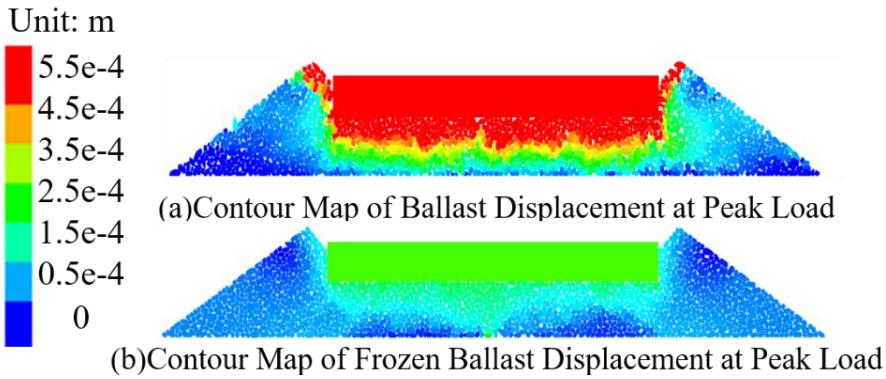

Figure 11: Contour Plots of Normal Ballast and Frozen Ballast at Load Peak

Figure 12 illustrates the subgrade loading characteristics under unfrozen and frozen ballast conditions. The results reveal that:

(1) Granular Ballast Bed: The subgrade is protected primarily through stress diffusion. In the unfrozen state, particle rearrangement and inter-particle friction facilitate the gradual downward spreading of concentrated loads, resulting in a broad stress distribution with a gentle gradient. Maximum stresses are confined to the shallow layer beneath the sleeper, while forces in the deep subgrade attenuate significantly. This demonstrates the granular bed's capacity for effective stress attenuation and protection.

(2) Frozen Ballast Bed: Increased stiffness inhibits particle motion, leading to a highly concentrated stress core beneath the sleeper. Loads transfer in a narrow columnar pattern with reduced spreading angles, penetrating deeply into the subgrade. Stress contours reveal elevated stress levels in the deep subgrade, particularly at the sleeper center where maximum stresses extend to the mid-to-lower layers. This vertical penetration mode undermines the ballast bed's original buffering and dispersion capabilities.

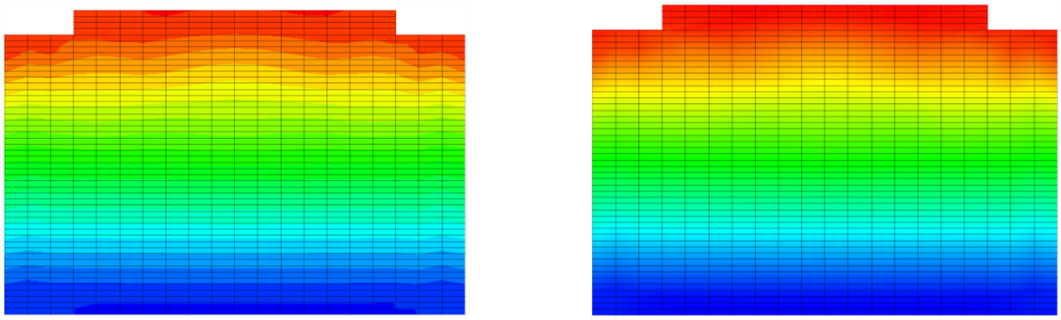

(a)Pressure Distribution in Subgrade under Load (b)Pressure Distribution in Frozen Subgrade under Load

Figure 12: Distribution Diagram of Subgrade Pressure under Load in Unfrozen and Frozen States

IV CONCLUSION

A refined two-dimensional coupled DEM–FDM model was established to investigate the dynamic response and mesoscopic load-transfer mechanisms of ballasted track-subgrade systems in seasonally frozen regions under varying train speeds and ballast ice contents. Based on the numerical analyses, the following conclusions can be drawn:

(1) Train speed and ice content exhibit significant coupled effects on the macroscopic dynamic response of the ballast-subgrade system. Vertical displacement amplitudes increase nonlinearly with train speed, particularly when the speed exceeds 160 km/h, while increasing ice content effectively suppresses ballast deformation by enhancing interparticle bonding and global structural stiffness. The freezing effect is more pronounced in deep and peripheral regions of the ballast bed.

(2) Freezing fundamentally changes the internal load-transfer mechanism of the ballast bed. In the unfrozen state, the ballast assembly transfers loads through flexible particle rearrangement and diffusive force-chain propagation, forming a broad trapezoidal stress distribution. Under frozen conditions, ice bonding restricts particle sliding and transforms the ballast skeleton into a rigid force-chain network, causing stress concentration beneath the sleeper and promoting columnar load penetration into the subgrade.

(3) Both vertical and lateral dynamic stresses of the subgrade increase with train speed and ice content, although train speed remains the dominant influencing factor. Vertical stress exhibits a characteristic "central-high, peripheral-low" distribution and is approximately 6–8 times larger than the lateral stress within the core loading zone. Freezing significantly enhances stress transmission efficiency, particularly in deep and peripheral regions, thereby increasing the risk of stress concentration and structural deterioration in the subgrade.

(4) From an engineering perspective, frozen ballast beds exhibit enhanced stiffness and load-bearing capacity, but simultaneously weaken the original stress diffusion and vibration attenuation functions of granular ballast. Therefore, in seasonally frozen regions, particular attention should be paid to the dynamic stress concentration beneath rail seats and within deep subgrade layers under high-speed operating conditions.

REFERENCES

[1]. Fan Z C 2012 Analysis of vertical dynamic characteristics of elastic long-sleeper ballastless track on simply supported beam bridge Thesis Central South University.

[2]. Wang J J, You R L, Du X G et al 2013 Selection analysis of ballastless track structure in heavy-haul railway tunnel Rail. Constr. 2013 132–6.

[3]. Lim W L, Mcdowell G R, Collop A C. The application of Weibull statistics to the strength of railway ballast [J]. Granular Matter, 2004, 6: 229-37.

[4]. Yan Y, Zhao C F, Li Y J, et al. Discrete element analysis of crushing characteristics of railway ballast [J]. Chinese Journal of Computational Mechanics, 2017, 34(05): 615-22.

[5]. Li X, Yan Y, Xue Y Z et al 2023 Three-point bending test study of frozen ballast aggregate under influence of ice content J. Exp. Mech. 38 47–56.

[6]. Wang Q Z, Liu J K, Tian Y H et al 2015 Orthogonal test study on frost heave of graded crushed stone in cold regions Rock Soil Mech. 36 2825–36.

[7]. Liu J, Wang P, Liu G, et al. Uniaxial compression characteristics of railway ballast combined with ice[J]. Construction and Building Materials, 2020, 263:120554.

[8]. Bian W, Ma Y, Wang Z. Dynamic Analysis of Freezing Railway Ballast Using the Discrete Element Method[J]. Geotechnical and Geological Engineering,2025,43(2):88-88.
[9]. Nurmikolu A. Fouling and frost susceptibility of railway ballast and subballast, field and laboratory study[M]. 2010.
[10]. Liu J X, Liu K, Liu Z Y et al 2025 Macro-mesoscopic resistance characteristics of frozen ballasted bed in plateau mountain railway J. China Rail. Soc. 47 153–9.
[11]. Bian W, Ma Y and Wang Z 2025 Dynamic analysis of freezing railway ballast using the discrete element method Geotech. Geol. Eng. 43 88.
[12]. Li Y P 2025 Study on settlement characteristics of ballasted bed under low-temperature freezing conditions Thesis Dalian Jiaotong University.
[13]. Chen X M, Chen N, Wang R J, Zhang X M and Wang W D 2021 Study on influence of train speed on working performance of ballasted bed based on discrete element method J. Rail. Sci. Eng. 18 2047–54.
[14]. Ren J, Dong J, Zhang K et al 2024 Transfer relation between subgrade frost heave and slab track deformation and vehicle dynamic response in seasonally frozen ground J. Zhejiang Univ.-Sci. A 25 130–46.
[15]. Bian W, Ma Y, Chen Z et al 2026 Influence of subgrade frost heave on ballasted track dynamics via a hybrid DEM-vehicle model Cold Reg. Sci. Technol. 246 104861.
[16]. TB/T 2034-1988 1988 Railway track strength inspection algorithm Standard.
[17]. Aursudkij B, McDowell G R and Collop A C 2009 Cyclic loading of railway ballast under triaxial conditions and in a railway test facility Granul. Matter 11 391–40.
[18]. Ministry of Railways of the People's Republic of China 2013 Technical code for dynamic acceptance of high-speed railway engineering TB 10761-2013 Standard Beijing: China Railway Publishing House.